HHS Public Access

Author manuscript

*Nat Neurosci*. Author manuscript; available in PMC 2014 June 01.

Published in final edited form as:

*Nat Neurosci*. 2013 December ; 16(12): 1764–1772. doi:10.1038/nn.3569.

# Regulation of interneuron excitability by gap junction coupling with principal cells

**Pierre F. Apostolides**[1,2] and **Laurence O. Trussell**[2]

[1]Neuroscience Graduate Program, Oregon Health & Science University, Portland, Oregon, 97239, USA

[2]Vollum Institute & Oregon Hearing Research Center, Oregon Health & Science University, Portland, Oregon, 97239, USA

## Abstract

Electrical coupling of inhibitory interneurons can synchronize activity across multiple neurons, thereby enhancing the reliability of inhibition onto principal cell targets. It is unclear whether downstream activity in principal cells controls the excitability of such inhibitory networks. Using paired patch-clamp recordings, we show that excitatory projection neurons (fusiform cells) and inhibitory stellate interneurons of the dorsal cochlear nucleus form an electrically coupled network via connexin36-containing gap junctions. Remarkably, stellate cells were more strongly coupled to fusiform cells than to other stellate cells. This heterologous coupling was functionally asymmetric, biasing electrical transmission from principal cell to interneuron. Optogenetically-activated populations of fusiform cells reliably enhanced interneuron excitability and generated GABAergic inhibition onto postsynaptic targets of stellate cells, whereas deep afterhyperpolarizations following fusiform cell spike trains potently inhibited stellate cells over several hundred milliseconds. Thus, the excitability of an interneuron network is bi-directionally-controlled by distinct epochs of activity in principal cells.

## Introduction

Cerebellum-like structures of vertebrates are thought to act as adaptive filters of ongoing sensory information, reducing the salience of predictable sensory input patterns[1–3]. The principal efferent neurons of these circuits integrate two types of excitatory synapses: “Instructive” signals from a specific sensory modality and “predictive” signals from other brain nuclei that convey the multisensory context in which the instructive signal occurred. Although these basic anatomical motifs are conserved across most cerebellum-like structures, the cellular mechanisms and local computations underlying the adaptive filtering of sensory information remain poorly understood[1].



Author Contributions:

P.F.A. collected the data. Both authors designed the study, analyzed and interpreted the results, and wrote the manuscript.

The dorsal cochlear nucleus (DCN) is an auditory brainstem region thought to function as an adaptive filter to cancel predictable, self-generated sounds[3,4]. Similar to other cerebellum-like structures, the DCN is divided into instructive and predictive pathways which converge upon principal neurons[1,3], an anatomical layout suggesting that auditory and multisensory information are processed by non-overlapping circuits. The glutamatergic principal neurons (termed fusiform or pyramidal cells) integrate sound frequency information from tonotopically-organized, auditory nerve synapses with multisensory signals relayed by granule cell parallel fibers (Fig. 1a). The parallel fiber pathway also recruits two types of inhibitory interneurons in the DCN's molecular layer: Purkinje-like cartwheel cells and superficial stellate cells that are analogous to the stellate/basket cells of the cerebellum[4]. Although fusiform cells receive convergent excitation from multisensory parallel fibers and the auditory nerve, the inhibitory stellate and cartwheel interneurons of the molecular layer only receive parallel fiber input. This suggests that while multisensory signals may filter auditory inputs by recruiting interneurons to modify fusiform cell spiking[5], auditory nerve synapses do not directly control the activity of molecular layer interneurons.

We find that the GABAergic stellate interneurons of the molecular layer are electrically coupled to the excitatory fusiform cells that integrate auditory and multisensory inputs. This novel circuit motif is surprising, as electrical coupling in the brain occurs primarily between inhibitory neurons of the same anatomical and functional class[6,7]. These heterologous electrical synapses showed directional asymmetry, thereby favoring transmission from the auditory to the multisensory processing domains. Accordingly, the functional consequences of electrical coupling were such that stimulating auditory nerve synapses onto fusiform cells reliably depolarized stellate cells, and fusiform cell activity was sufficient to generate robust inhibition in the multisensory pathway. Our data significantly revise the connectivity map of DCN, and show that at the first synapses of the central auditory system, interneuron excitability is temporally controlled by the activity of projection neurons via electrical synapses.

## Results

### Electrical coupling between interneurons and principal cells

We made whole-cell current-clamp recordings from pairs of fusiform and stellate cells in DCN-containing brain slices from 15–32 day-old mice. Neurons were identified based on morphological and electrophysiological criteria (see *Methods*). In 92/203 attempted pairs (45%), hyperpolarizing one neuron (the "prejunctional" cell) via negative current injection caused a simultaneous hyperpolarization in the other cell (the "postjunctional" cell; Figure 1b). The bi-directional translation of negative, subthreshold membrane potential deflections across two neurons is a hallmark of electrical coupling[6].

For 57 pairs in which transmission was tested bi-directionally, we calculated a coupling coefficient, defined as the ratio of the mean hyperpolarization during the last 50–100 ms of the current step in postjunctional and prejunctional cells. Surprisingly, we found that coupling strength showed strong directional preference, such that the average coupling coefficient in the fusiform-to-stellate direction was 0.10±0.01, but only 0.026±0.003 in the stellate-to-fusiform direction (Fig. 1c, d). Although electrical coupling is stronger in

neonates in some brain regions[8,9], coupling remained robust in DCN slices from mice 7–9 weeks of age (connection probability: 10/16; 62.5%). For pairs recorded in more mature animals, the average fusiform-to-stellate cell coupling coefficient was 0.13±0.04 (n=8 pairs tested in this direction), whereas the stellate-to-fusiform coupling coefficient was 0.026±0.005 (n=5 pairs tested). These results show that the excitatory projection neurons of the DCN form strong, developmentally-persistent electrical synapses with local inhibitory interneurons. Furthermore, the directional asymmetry is such that coupling from fusiform-to-stellate cells is nearly 4-fold stronger than in the opposite direction. Using the approach of Bennett (1966)[10] we also calculated the junctional conductances for each direction, finding an average fusiform-to-stellate cell conductance of 0.41±0.04 nS, and stellate-to-fusiform conductance of 0.98±0.11 nS (n=57 pairs; see Methods).

## Electrical coupling requires Cx36-containing gap junctions

Similar to other brain regions[6], electrical coupling was significantly compromised in DCN slices from mutant mice lacking the neuronal gap junction protein connexin36 (Cx36−/− mice; Fig. 1d). Only 3/60 attempted pairs were coupled in these mice ($\chi^2(1)=30.9$, $p<0.0001$ compared to wild-type). The average fusiform-to-stellate coupling coefficient of the remaining coupled pairs was 0.024±0.012 (n=3), whereas coupling was 0.003±0.001 in the opposite direction (n=2). Furthermore, electrical coupling in wild-type mice was blocked by a 15–30 min bath application of the gap junction blocker meclofenamic acid (MFA; Supplemental Fig. 1). Together, these data show that electrotonic coupling between fusiform and stellate cells reflects electrical synapses between two different cell types, and that this coupling requires connexin36.

These results are surprising, as electrical coupling in the brain is typically observed between neurons of the same class[7,11]. We therefore asked how coupling between fusiform and stellate cells contrasts with the efficacy of electrical transmission between the same cell types. Electrical coupling was indeed found to occur between stellate cells (9/42 of attempted pairs, Supplemental Fig. 2a), as predicted from an anatomical study in the DCN[12], and by homology to cerebellar stellate cells[13] (Supplemental Fig. 2b). However, the homologous coupling between stellate cells (0.024±0.005, average of both directions) was much weaker than fusiform-to-stellate cell coupling. Interestingly, we also found electrical coupling in the majority of attempted fusiform cell pairs (20/28; Supplemental Fig. 3), although again this coupling was weak (0.014±0.001). By contrast, we found no evidence for electrical coupling between fusiform cells and another major molecular layer interneuron, cartwheel cells (0/27 connected pairs, data not shown). This result highlights a strong specificity of electrical coupling in the DCN, as cartwheel cells make potent inhibitory synapses onto fusiform cells and overlap extensively in their dendritic fields[4]. Altogether, our data reveal a broad, cell-type specific network of gap junction-mediated communication between excitatory and inhibitory neurons in the DCN molecular layer, and show that electrical transmission is largely biased towards heterologous coupling in the fusiform-to-stellate cell direction.

### Propagation of fusiform spikes into stellate cells

Previous studies show that fusiform cells fire spontaneously *in vitro*[5,14] and *in vivo*[15]. The strong coupling between fusiform and stellate cells suggests that these spikes could modulate the membrane potential of electrically-coupled stellate cells. Accordingly, we observed spontaneous, subthreshold spikelets in the majority of current-clamp recordings from single stellate cells (44/65; 67%. Fig. 2a, top trace). In voltage clamp, spikelets were clearly biphasic, with a fast inward current followed by a slower, smaller outward current (Fig. 2a, bottom trace). These events were due to electrical coupling as they occurred in the presence of glutamate, $GABA_A$, and glycine receptor antagonists and were absent in recordings from *Cx36*−/− mice (Fig. 2b). Furthermore, paired recordings revealed that action potentials in prejunctional fusiform cells evoked spikelets in the postjunctional stellate cell (Fig. 2c). Spikelets had an average positive peak amplitude of 0.9±0.2 mV and a mean latency from the peak of the prejunctional spike to that of the postjunctional spikelet of 837±72 μs (n=11 pairs). Figure 2d illustrates a fusiform cell spike-triggered average of action potential-evoked spikelets from the same pair as in Figure 2c. Furthermore, we never observed spikelet transmission failures, indicating that fusiform cell spikes reliably propagate to stellate cells.

Stellate cell somata lie primarily near the DCN ependyma[12], suggesting that electrical synapses are located in fusiform cell apical dendrites. In a subset of our paired recordings, we investigated the location of putative contacts by first visualizing the morphology of fusiform cells with a fluorophore (Alexa488 or Alexa594) in the pipette internal solution and then selectively targeting stellate cells located near the fusiform cell's apical dendrites. This method significantly increased the probability of finding an electrically coupled pair from 36% without *a priori* visualization of fusiform cell morphology (41/113) to 57% when we targeted stellate cells near fusiform cell dendrites (51/90. $\chi^2(1)=7.6$, p=0.006). We further characterized the anatomical organization of electrical coupling by imaging connected pairs using 2-photon microscopy. Fusiform and stellate cells were filled with Alexa488 (90 μM) and Alexa594 (20–30 μM) dyes, respectively. Figure 3a shows a Z-projection of the paired recording in Figure 1b, with the dashed line denoting the ependymal border. We consistently (n=11 electrically-coupled pairs) observed that stellate cell processes were primarily (though not exclusively) restricted to the distal region of fusiform cell apical dendrites, in agreement with previous work[12]. Moreover, the dendritic arbors of the two cell types could be in close apposition (Fig. 3 ii–iii), suggesting putative points of contact.

Previous studies suggest that action potentials in fusiform cells back-propagate into the apical dendrites[16,17]. The slower waveform of the spikelet versus the fusiform cell action potential suggests that the latter may be filtered as it propagates to the stellate cell, although the lack of transmission failures argues that fusiform cell spikes nevertheless reliably propagate through the apical dendrites (Fig. 2c, d). In agreement with this interpretation, 2-photon $Ca^{2+}$ imaging of fusiform cells loaded with Alexa594 and the $Ca^{2+}$ indicator Fluo5F (150–200 μM) revealed that action potentials invaded the entire apical arbor (Fig. 3b, c). As expected from back-propagation of action potentials, the absolute amplitude of action potential-evoked ΔG/R signal (see *Methods*) did not attenuate as a function of approximate distance from the soma, but remained constant throughout the distal processes (n=6 cells,

Fig. 3c). Altogether these data argue that spikelets in stellate cells originate as action potentials that have propagated through the apical dendritic arbor of the fusiform cell. Moreover, the obvious size difference between fusiform and stellate cells suggests that impedance mismatch contributes to the coupling asymmetry observed in Figure 1. Accordingly, input resistances for the two cells were found to differ by over tenfold (fusiform cells: 87±37 MOhms [cf. reference 18]; stellate cells: 996±139 MOhms (n=29), this study).

## Frequency-dependence of transmission

Previous studies suggest that spikelets may exert a predominantly inhibitory effect on the postjunctional cell, as the low-pass filter properties of gap junction channels allow preferential passage of the spike after-hyperpolarization (AHP) compared to the faster depolarizing $Na^+$ upstroke[19,20]. Indeed, our paired recordings (Fig. 2d) show that fusiform-to-stellate cell spikelets are biphasic, with a prominent negative-going phase. However, other studies indicate that the shape of postjunctional spikelets depends on the firing rate of the prejunctional cell, and that the hyperpolarizing trough disappears at frequencies >50 Hz[21]. We therefore asked if the prejunctional spike frequency determined whether fusiform cells exert a net depolarizing or hyperpolarizing effect on stellate cells. We evoked spikes in fusiform cells at different frequencies and measured the mean change in membrane potential of the stellate cells to which they were coupled (Fig. 4a, b). Stellate cells were hyperpolarized with constant bias current to prevent action potentials. Fusiform cell spikes evoked at 1 and 10 Hz had no effect on mean membrane potential in stellate cells (1 Hz: 0.005±0.009 mV; 10 Hz: −0.04±0.04 mV, n=9 pairs). Thus, during low-frequency activity similar to that observed *in vivo* during periods of quiescence, fusiform cell activity does not cause the stellate cell's membrane potential to appreciably deviate from baseline. On the other hand, high-frequency fusiform cell activity (50 and 100 Hz) had a net excitatory effect, causing a mean voltage change of +0.3 mV±0.1 mV and +0.8±0.2 mV. Given that fusiform cells can fire >200 Hz during sound-evoked activity *in vivo*[15,22], these data indicate that physiological spike rates in single fusiform cells depolarize the membrane potential of electrically coupled interneurons in a frequency-dependent manner.

Following a spike train in fusiform cells, a post-train AHP was invariably apparent. For trains elicited by square-pulse current injection (0.3–1 nA, 0.4–1 s), the negative peak of the AHP was −11.3±1.0 mV below rest with a half-width of 406± 58 ms (n=8 fusiform cells; Fig. 4c). Intracellular recordings from fusiform cells driven by acoustic stimuli *in vivo* show that this AHP occurs upon sound termination[23,24], indicating that the AHP is not an artifact of direct current injection through the recording pipette. Paired recordings revealed that the post-train AHP in fusiform cells reliably invaded stellate cells (n=7 pairs, Fig. 4c). Interestingly, the absolute peak amplitude of the postjunctional AHP in stellate cells was 92±8% of the steady-state depolarizing phase, suggesting that positive and negative-going phases of fusiform cell activity may be of comparable significance to stellate cells.

## Auditory nerve activity is transmitted to stellate cells

Auditory nerve fibers contact the basal dendrites of fusiform cells, but do not extend into the DCN molecular layer[25]. However, the results of Figures 4a–c show that single fusiform cells

can control the membrane potential of electrically-coupled stellate cells, suggesting that acoustic information from the auditory nerve may nevertheless reach stellate cells through electrical synapses. We explicitly tested the possibility that stellate cells sense activity in the auditory pathway by recording from single stellate cells and stimulating the auditory nerve with a bipolar electrode placed in the ventral cochlear nucleus. In agreement, trains of stimuli to the auditory nerve depolarized stellate cells (3.2±0.5 mV; n=6 cells, Fig. 4d, e). Two features of this response indicate that it occurred through gap junction coupling with fusiform cells. First, the depolarization was followed by a hyperpolarization (in current clamp) or outward current (in voltage clamp; Fig. 4d), similar to the postjunctional activity generated by direct current injection in fusiform cells (Fig. 4c). The slow outward current seen in voltage-clamp likely reflects the membrane potential of prejunctional fusiform cells relaxing towards baseline during the decay of the AHP. Second, depolarization of the stellate cell to 0 mV (recorded with a Cs-based internal solution), which markedly reduces the driving force for glutamatergic transmission, only mildly reduced the amplitude of the steady-state response (Fig. 4e; average amplitude at −67 mV: −17±3 pA; 0 mV: −13±3 pA; ratio of average current at 0 mV to −67 mV= 0.75±0.03; n=5 cells). Nevertheless, these voltage-independent responses were entirely blocked by bath application of AMPA and NMDA receptor antagonists (Fig. 4e, lower traces; n=3 cells), showing that they were generated by glutamatergic synaptic transmission. Thus, auditory nerve synapses generate excitatory responses that do not arise from transmitter-gated channels in stellate cells. These results strongly suggest that the auditory pathway transmits information to stellate cells, albeit independently of a direct auditory nerve projection into the molecular layer.

### Optogenetic activation of multiple fusiform cells

Because auditory nerve input to the DCN is tonotopically organized, single fusiform cells respond best to a limited range of sound frequencies. If multiple prejunctional fusiform cells with similar frequency tuning converge upon a single stellate cell, our paired recordings likely underestimate the extent to which electrical synapses may control stellate cell excitability. To determine the capacity of multiple prejunctional fusiform cells to control the stellate cell membrane potential, we performed experiments in transgenic mice expressing the light-activated cation channel channelrhodopsin2 (ChR2) driven by the Thy1 (*Thy1-ChR2-YFP* line 18[26]) or vesicular glutamate transporter 2 promoters (*VGluT2-ChR2-YFP*[27]). Both lines robustly expressed ChR2 in fusiform cells: Blue light flashes delivered through the microscope objective caused large inward currents in voltage-clamped fusiform cells and reliably drove spiking in current-clamp (Fig. 5a, d). The absolute amplitudes of photocurrents in voltage-clamped fusiform cells from *Thy1-ChR2* mice were on average significantly larger than those observed in *VGluT2-ChR2* line (Thy1: 991± 185 pA, n=19 cells. VGluT2: 225±25 pA, n=13 cells. t(30)=3.4, p=0.002, unpaired t-test) However, similar results were obtained with Thy1 and VGluT2 lines for the optogenetic experiments in Figures 5–7, so the data were pooled.

In slices from ChR2 mice, blue light also robustly increased the firing frequency of stellate cells recorded in current-clamp (Fig. 5b, e). These experiments were performed in the presence of AMPA and NMDA receptor blockers (10 μM NBQX and 5 μM R-CPP), showing that the rapid increase in stellate cell spike rate was not due to ChR2 activation of

presynaptic glutamatergic axons. We further investigated the depolarization underlying this phenomenon by hyperpolarizing stellate cells with negative bias current to prevent spiking. As expected from activating prejunctional fusiform cells, blue light evoked trains of spikelets atop a DC depolarization (Fig. 5c, f, upper traces) followed upon light termination by the post-train AHP seen in paired recordings (e.g., Fig. 4c). In voltage-clamped stellate cells, the same light stimuli caused biphasic "postjunctional photocurrents" characterized by spikelets riding atop an inward current, followed by a slow outward current upon light termination (Fig. 5c, f, lower traces). The amplitudes of the mean steady-state inward and peak outward postjunctional photocurrents were −16.9±2.5 and 14.4±1.8 pA, respectively (n=28 cells). Careful inspection of the voltage-clamp traces revealed spikelets of different amplitudes (Fig. 5f, g), suggesting that multiple fusiform cells with different coupling coefficients contact a single stellate cell. Additionally, we never observed light-evoked spikelets, depolarizations or inward currents in cartwheel cells (0/37 cells tested), further highlighting the cell-type specificity of electrical coupling.

Several control experiments led us to reject the possibility that the light-evoked depolarizations and postjunctional photocurrents in stellate cells were due to direct ChR2 expression in the stellate cell plasma membrane. First, the VGluT2 line should show ChR2 expression restricted to excitatory glutamatergic neurons such as fusiform cells[28] and not in the GABAergic stellate cells[29]. Second, if postjunctional photocurrents are due to ChR2 expression in stellate cells, they should follow the current-voltage (IV) curve documented in previous studies of the ChR2 cation channel and reverse at positive potentials[30]. However, postjunctional photocurrents in voltage-clamped stellate cells were only minimally voltage-dependent and remained inward at +53 mV, as expected for a cation current arising through an unclamped distal compartment (Supplemental Fig. 4a, b). By contrast, photocurrents in fusiform cells displayed a rectifying IV relationship expected of the ChR2 channel and reversed at positive potentials. Third, the gap junction blocker MFA abolished postjunctional photocurrents in stellate cells but had little effect on ChR2 photocurrents in fusiform cells (Supplemental Fig. 4c, d). Together, these data show that postjunctional photocurrents represent the summed activity of prejunctional fusiform cells, not ectopic expression of ChR2 in stellate cells. Finally, bath application of tetrodotoxin (TTX; 500 nM) significantly reduced the amplitude of the stellate cell postjunctional depolarization by 38±4% (baseline: 5.8± 1.0 mV, TTX: 3.4±0.6 mV, n=14. $t(13)=4.6$, $p=0.0005$, paired t-test), and reduced the postjunctional AHP during the light-off response by 61±3% (baseline: −5.2± 0.8 mV, TTX: −2.2± 0.5 mV, n=14. $t(13)=6.96$, $p<0.0001$, paired t-test). These data indicate that spikes in prejunctional fusiform cells contribute to the light-evoked depolarizations in stellate cells. Thus, active and passive depolarizations in fusiform cells are transmitted to stellate cells. Moreover, the fact that the ChR2-induced, TTX-sensitive depolarization (2.4 mV) in stellate cells was over 2-fold greater than the depolarization generated by stimulating a single fusiform cell (0.8 mV at 100 Hz) indicates that the ChR2-induced depolarization was indeed generated by multiple prejunctional fusiform cells.

## Fusiform cells control stellate cell spike output

Can a single fusiform cell suffice to increase stellate cell spike output, or does this require simultaneous activity in multiple prejunctional cells? We recorded electrically-coupled pairs

and injected a family of depolarizing current steps in the stellate cell with and without simultaneous 100-Hz activity in the prejunctional fusiform cell (Fig. 6a). Negative bias current was used to prevent spontaneous firing of both neurons. A linear fit was made to the non-zero portions of stellate cell input/output curves to compare the slope and offset (x-intercept for y=0) of the function during the two conditions[31]. In 8 pairs tested, fusiform cell activity shifted the offset of stellate cell input/output curves from 28.8± 5.0 pA during baseline to 25.2± 5.0 pA when the fusiform cell was active (Fig. 6c; −13± 4% difference. t(7)=3, p=0.02, paired t-test). However, fusiform cell activity had no significant effect on the slope of the input/output curve (baseline: 1.1±0.1 pA/Hz, with fusiform cell activity: 1.2±0.1 pA/Hz. +4.5±2.8% change. t(7)=1.53, p=0.14, paired t-test). Furthermore, activating multiple prejunctional fusiform cells with blue light stimuli in ChR2 mice (Fig. 6b) caused significantly larger shifts in the offset of stellate cell input/output functions (Fig. 6d; from 34.1± 5.4 pA to 15.1± 4.9 pA; −52± 10% difference. n=10 cells, t(9)=3.66, p=0.005, paired t-test) with no significant change in the slope (1.6±0.15 pA/Hz to 1.47± 0.11 pA/Hz, −6.8±4.3% change. t(9)=1.34, p=0.21, paired t-test). Thus, activity in even a single fusiform cell significantly enhances the excitability of local interneurons, and this represents a largely additive transformation of the stellate cell's input/output function.

The large postjunctional AHP observed in stellate cells following fusiform cell or auditory nerve spike trains (Fig. 4 & 5) suggests that the timing of fusiform cell activity determines whether electrical synapses exert a net excitatory or inhibitory effect on stellate cell spike output. We tested this by recording single stellate cells in ChR2 mice and varying the time interval between depolarizing current steps in the stellate cell and blue light stimuli, thereby allowing either the depolarizing or AHP phase of fusiform cell activity to overlap with stellate cell spiking (Fig. 7a). The results were dramatic, as coincident activation of fusiform cells within a ±100 ms time window of stellate cell depolarization increased spike output by 50±5% compared to baseline (Fig. 7b, n=13). By contrast, activating fusiform cells 500 ms *before* stellate cell current injection, resulting in maximal overlap of the postjunctional AHP and stellate cell depolarization, reduced the total number of spikes by 53±6%. Thus, the timing of fusiform cell activity with respect to stellate cell excitation bi-directionally regulates the number of spikes generated by the interneuron over a 3-fold range.

## Fusiform cell activity generates local inhibition

Our data show that activity of even a single prejunctional fusiform cell is sufficient to excite stellate cells, and thus predict that fusiform cell spiking should increase inhibition in the DCN molecular layer by depolarizing the stellate cell network. By homology to their cerebellar counterparts, stellate cells are suggested to synapse onto the Purkinje-like cartwheel cells of the DCN[12,32]. Accordingly, paired recordings revealed unitary stellate-to-cartwheel cell inhibitory postsynaptic currents (IPSCs) in 8/26 attempted pairs (30.8% connection probability, Fig. 8a).

To explicitly test whether fusiform cell activity generates inhibition in the DCN, we recorded from single cartwheel cells and optogenetically activated fusiform cells (300–500-ms light stimuli). In the majority of voltage-clamped cartwheel cells (25/28), optogenetic activation of fusiform cells triggered barrages of IPSCs (Fig. 8b) that were entirely blocked

by the $GABA_A$ receptor antagonist SR95531 (5 μM; Fig. 8b, n=8). These IPSCs were not due to polysynaptic recruitment of interneurons via glutamatergic synapses because excitatory transmission was blocked by 10 μM NBQX and 5 μM R-CPP in all experiments.

We also examined whether activation of fusiform cells could lead to inhibition of other fusiform cells through stellate-to-fusiform chemical synapses. Fusiform cells from *VGluT2-ChR2* mice were recorded in voltage-clamp near the reversal potential for the ChR2 photocurrent (0–13 mV) using a Cs-based internal solution. In 7 of 11 cells tested, blue light stimuli generated barrages of IPSCs that were partially occluded by the small inward photocurrent (Fig. 8c). These IPSCs were not triggered by excitatory glutamatergic synapses because all experiments were performed in the presence of NBQX and R-CPP. Bath application of inhibitory synaptic blockers (SR95531 and strychnine; n=6 cells) blocked the IPSCs, and subsequent digital subtraction of the average photocurrent trace from the single traces recorded in NBQX/CPP clearly showed that activation of neighboring fusiform cells generated a robust inhibitory response in the voltage-clamped neuron (Fig. 8d). Thus, principal neuron activity generates time-locked increases in local inhibition, thereby regulating the excitability of neighboring principal neurons and interneurons.

## Discussion

A hallmark of sensory circuits is that external stimuli recruit inhibition proportional to the magnitude of excitatory drive[33]. Whether the sensitivity of inhibitory neurons is fixed or labile with respect to a given stimulus is unclear. We have demonstrated a simple cellular mechanism that uses gap junctions to rapidly control the moment-to-moment dynamics of inhibition based upon the timing of principal neuron activity. The probability of electrical coupling between principal cells and interneurons was high (57%), suggesting that this transmission pathway constitutes a significant component of the DCN circuit. Moreover, electrical coupling was robust in animals as old as two months postnatal, indicating that this circuit motif should function as a component of sensory processing and is not a transient developmental phenomenon. Thus, our findings raise the possibility that even at the earliest stages of auditory processing, ongoing sensory input bi-directionally regulates the threshold for recruiting local inhibition.

These results significantly revise the canonical DCN model, whereby multisensory and auditory inputs recruit distinct classes of interneurons[4]. Through electrical coupling with fusiform cells, the stellate cell membrane potential will rapidly sense ongoing auditory activity, a prediction supported by our observation that auditory nerve activation itself generates signals in stellate cells through gap junction coupling. There are no recordings from identified stellate cells *in vivo*, presumably due to their small size and precarious location at the ependymal edge of the brainstem. Given that single stellate cells are coupled to multiple prejunctional fusiform cells, our data suggest that electrical coupling may endow stellate cells with complex “best frequency” characteristics reflecting the additive frequency tuning properties of prejunctional fusiform cells. Nevertheless, an understanding of how electrical coupling regulates information flow through the DCN will require knowing the functional connectivity between a stellate cell’s postsynaptic targets and its electrically-coupled partners. Stellate cells form inhibitory synapses onto cartwheel and fusiform

cells[32,34] (Fig. 8). Activating stellate cells through the gap junction pathway generated IPSCs in a functionally silent (e.g., voltage-clamped) fusiform cell (Fig. 8c, d), showing that stellate cells do not strictly perform feedback inhibition onto activated principal neurons. However, it is unknown whether stellate cells inhibit fusiform cells that are tuned to similar frequencies as those with which they form electrical synapses, or if stellate cells inhibit fusiform cells across frequencies (i.e., lateral inhibition). Similarly, the spatial distribution of cartwheel cell axons is not yet known, and it remains to be determined if stellate cells inhibit cartwheel cells that control local or more distant fusiform cells.

Further studies are required to definitively assign a specific functional role for the novel circuit we have identified. The DCN is organized similarly to the cerebellum and cerebellum-like structures found in mammals and weakly electric fish: Fusiform cells are analogous to deep cerebellar nucleus neurons and the glutamatergic efferent cells of mormyrid electric fish's electrosensory lobe, whereas cartwheel cells are thought to function as the Purkinje-like cells of these circuits[1,4]. Given that cerebellum-like circuits may mediate the adaptive filtering of self-generated sensory input, the molecular layer circuitry of the DCN could facilitate comparison of acoustic signals in the environment with body orientation or activity[3,4]. A key cellular phenomenon suggested to underlie such adaptive filtering is that coincident activity of predictive parallel fiber and instructive sensory pathways induces an anti-Hebbian, long-term depression of the active parallel fiber synapses[35,36]. For example, in the electrosensory lobe of the mormyrid electric fish, the Purkinje-like medium ganglion cells and excitatory efferent neurons integrate sensory information from electroreceptors on the skin (e.g., instructive signals) with parallel fiber synapses that convey predictive information regarding the fish's motor movements and behavior[1,3]. Simultaneous pairing of motor commands with electrosensory signals leads to long-term depression of the active parallel fibers in Purkinje-like cells and efferent neurons[37,38]. On a circuit level, this phenomenon is thought to be involved in generating activity patterns that are "negative images" of predictable sensory input [1,3]. However, experiments show that associative, long-term plasticity in cerebellum-like circuits requires prolonged induction protocols and is fully expressed only several minutes after induction[17,36,39,38]. Our work suggests an alternative mechanism that might contribute to a moment-to-moment reduction of parallel fiber synapses, thereby mediating adaptation to a rapidly changing environment. We find that activation of fusiform cells via the auditory pathway depolarizes stellate cells (Fig. 4d), and thus can sensitize molecular layer interneurons to subthreshold parallel fiber inputs. Furthermore, fusiform cell activity alone is sufficient to generate robust inhibition onto two major targets of parallel fibers: Cartwheel cells and neighboring fusiform cells (Fig. 8). Thus, auditory signals could, in principle, rapidly recruit or suppress stellate cells and control the efficacy of parallel fiber activity, depending on the relative timing of auditory and non-auditory sensory signals. Interestingly, recent studies suggest that cerebellar stellate cells sense glutamate "spillover" from climbing fiber synapses[40,41,42,] and feedforward inhibition generated by climbing fiber activity is sufficient to rapidly decrease the capacity of parallel fibers to drive spikes in neighboring Purkinje cells[42]. Together with our data, these findings imply that transmission of instructive signals to molecular layer interneurons may be a general feature of cerebellum-like circuits.

# Methods

## DCN brain slice preparation

All procedures involving animals were approved by OHSU's Institutional Animal Care and Use Committee. C57/BL6 wild-type mice postnatal 15–32 days were used for the majority of the experiments. For optogenetic experiments, mice were *B6.Cg-Tg(Thy1-COP4/EYFP)18Gfng/J* (*Thy1-ChR2*; JAX stock # 007612) or *C57Bl/6-TG(Slc17a6-COP4*H134R/EYFP)2OKi/J* (*VGluT2-ChR2*; JAX stock # 017978). Mice were anesthetized by isofluorane inhalation, followed by decapitation, and 200–250 μm coronal DCN slices were cut in a cold sucrose solution containing (in mM) 87 NaCl, 25 $NaHCO_3$, 25 glucose, 75 sucrose, 2.5 KCl, 1.25 $NaH_2PO_4$, 0.5 $CaCl_2$, 7 $MgCl_2$, and bubbled with 5% $CO_2$/95% $O_2$. After cutting, slices recovered for 30–45 min at 34° C in an ACSF solution containing (in mM) 130 NaCl, 2.1 KCl, 1.7 $CaCl_2$, 1 $MgSO_4$, 1.2 $KH_2PO_4$, 20 $NaHCO_3$, 3 Na-HEPES, 10–12 glucose, bubbled with 5% $CO_2$/95% $O_2$ (300–310 mOsm). In some experiments, 5 μM R-CPP, 50 μM D-APV or 5 μM MK801 were added to the slice and recovery solutions. After recovery, slices were kept at room temperature (~22 C°) until recording.

For DCN slices from mature animals, P54–P63 mice were anesthetized with an i.p. injection of 2% Avertin, transcardially perfused and the brain sliced in a chilled solution containing (in mM) 93 NMDG, 2.5 KCl, 1.2 $NaH_2PO_4$, 30 $NaHCO_3$, 20 HEPES, 10 $MgSO_4$, 0.5 ascorbic acid, 2 thiourea, 3 Na-pyruvate, 25 Glucose, 0.5 $CaCl_2$, 0.005 MK801, 12 n-acetyl-l-cysteine, 300–310 mOsm, pH adjusted to 7.3–7.4 with HCl[43]. Slices recovered at 34° C in NMDG-based solution for 10–15 min followed by a 40–60 min recovery period at room temperature in standard ACSF.

## Electrophysiology

Slices were transferred to a recording chamber and continuously perfused at 3–4 ml/min with ACSF heated to 32–34 C° by an inline heater. Neurons were visualized by Dodt contrast optics with a 40x objective. Chemical synaptic transmission was blocked in most experiments in Figures 1–3 and 5–7 by adding (in μM) 10 NBQX, 5 R-CPP (or 50 D-APV or 5 MK801), 0.5–2 strychnine, 5–10 SR95531. 0.5–1 TTX was sometimes added to experiments in Figure 1 and Supplemental Figures 3 and 4 to stop spontaneous firing. For experiments in Figures 4d–e, NBQX and R-CPP were omitted to enable activation of auditory nerve synapses. Fusiform cells were identified by previously published criteria[5,44]. Superficial stellate cells were identified by their location at the ependymal edge of the DCN molecular layer and soma size[12]. Stellate cells could be easily distinguished from cartwheel cells by their smaller soma located at the ependymal edge of the DCN, stronger $I_h$ sag upon hyperpolarization, and significantly higher input resistances (stellate: 996± 139 MOhm, n=29. Cartwheel: 50± 4 MOhm, n=12. $t(39)=4.2937$, $p=0.0001$, unpaired t-test). In addition, 30 μM Alexa488 (or 20 μM Alexa594) was added to the pipette solution in many experiments to visualize the somatodendritic morphology. The pipette solution for most current- and voltage-clamp experiments contained (in mM) 113 K-gluconate, 4.8 $MgCl_2$, 4 ATP, 0.5 Tris-GTP, 14 Tris-phosphocreatine, 0.1 EGTA, 10 HEPES, pH 7.25 with KOH, ~290 mOsm. In some experiments in Figure 1, 15.5 KCl was substituted for equimolar K-Gluconate. For IV curves in Supplemental Figure 4, the internal solution contained (in mM)

64.5 $CsMeSO_3$, 30CsFl, 5 TEA-Cl, 5 QX314-Cl, 5 $Cs_4$BAPTA, 4.8 $MgCl_2$, 4 ATP, 0.5 GTP, 10 Tris-phosphocreatine, 10 HEPES. In some experiments, CsFl was replaced with 15 $CsMeSO_3$ and 15.5 CsCl. Data are corrected for experimentally-determined liquid junction potentials of 7 or 10 mV ($CsMeSO_3$ and K-Gluconate internal solutions, respectively). For paired recordings in Figure 8, 10 mM GABA was added to the presynaptic K-Gluconate solution to reduce transmitter washout during whole-cell dialysis[45], and cartwheel cells in Figure 8a, b were recorded with a Cs-based internal solution containing 103 CsCl in place of $CsMeSO_3$ and CsFl. Fusiform cells in Figure 8c, d were recorded with the $CsMeSO_3$ internal solution. Pipette resistances for fusiform/cartwheel and stellate cells were typically 2–3 and 3–5 MOhm, respectively. In current-clamp, pipette capacitance was canceled and bridge balance maintained. For voltage-clamp recordings, neurons were held between −60 and −80 mV. Series resistance (< 15 and 25 MOhm for fusiform/cartwheel and stellate cells, respectively) was compensated 60–80% 'correction', 90% 'prediction' (bandwidth=3 kHz) and experiments were discarded if series resistance varied more than 20–25%. Stimulation of auditory nerve fibers (50–100 μsec pulses, 0.5–5 V) was performed using a bipolar metal electrode positioned in the ventral cochlear nucleus in a coronal slice that contained both cochlear nuclear divisions. Optogenetic stimulation was performed as described in ref. 45 or using a custom-built, TTL-gated blue LED light source.

## 2-Photon imaging

The 2-photon imaging system (Prairie Technologies) is described in detail in reference 46. For $Ca^{2+}$ imaging experiments, EGTA in the K-Gluconate internal solution was replaced with 150–200 μM Fluo-5F and 20 μM Alexa594. A Ti:sapphire pulsed laser (Coherent Chameleon Ultra II) was set to 810 nm and line scans (2–2.4 ms) were performed at multiple sites along the somatodendritic axis of fusiform cells. Epi- and transfluorescence signals were collected with a 40x, 0.8 NA objective and a 1.4 NA oil immersion condenser. For imaging the morphology of coupled pairs, the laser was set to 800 nm; stellate and fusiform cells were filled with 20–30 μM Alexa594 or 90 μM Alexa488, respectively.

## Auditory Brainstem Response

In order to be assured that the Cx36 KO mice did not have gross abnormalities in auditory function, we measured auditory brainstem responses (ABR). Three KO and three wt mice (P30–33) were anesthetized with a ketamine/xylazine cocktail, their eyes coated with Altalube (15% mineral oil/85% white petroleum) to prevent drying, and then placed on a heating pad in a sound-proof chamber. The experimenter was blinded to the genotype of the animals. Needle electrodes were placed subcutaneously near the ear at the vertex, with reference electrodes placed at the level of scalp and thorax. Each ear was then stimulated separately with a closed tube sound delivery system sealed into the ear canal. The auditory brain-stem response to a 1-ms rise-time tone burst at 4, 8, 12, 16, 24, and 32 kHz was recorded, and thresholds for visually obvious peak 1 and 4 responses were obtained for each ear. Average thresholds were identical for wildtype and KO mice across all tested frequencies ($F(1,24)=0.0005$, $P=0.99$, two-way ANOVA).

### Data Acquisition and analysis

Electrophysiology data were recorded using Pclamp 9 software with a Molecular Devices Multiclamp 700B amplifier and a Digidata 1332A analog-to-digital converter board. Signals were acquired at 20–50 KHz and low-pass filtered at 1–10 KHz for offline analysis. $Ca^{2+}$ imaging experiments were analyzed using custom macros in ImageJ or Igor; data are expressed ΔG/R*100 and each trace is an average of 20–25 events. $Ca^{2+}$ transient amplitudes were calculated by extrapolating the peak from monoexponential fits to the fluorescence decay at the end of the action potential train.

Coupling conductances between cells were calculated according to equation 7 of ref. 10, which is based on current responses and estimates of input resistance. Although the results suggested directional rectification of gap junction conductance between fusiform and stellate cells, the high input resistance of stellate cells makes it difficult to estimate an input resistance independent of junctional resistances in the network. The equation also does not account for dendritic cable properties. These issues may account for the seemingly lower junctional conductance in the fusiform-to-stellate direction despite the higher coupling coefficient as compared to the stellate-to-fusiform direction. In any case it is likely that the tenfold high resistance of stellate cells is the dominant factor in greater efficacy of transmission from fusiform to stellate cells. Similar results were obtained using the equations of ref. 47.

### Statistics

Data were analyzed with statistical tests listed in the main text. For ANOVAs, alpha was corrected for multiple comparisons and individual comparisons were made using Dunnett's multiple comparisons test. $\chi^2$ tests were performed with Yate's correction. All errors given as s.e.m.

### Reagents

NBQX, R-CPP, D-APV, TTX, and SR95531 were from Abcam. Strychnine, MK801, and MFA were from Sigma-Aldrich.

## Supplementary Material

Refer to Web version on PubMed Central for supplementary material.

## Acknowledgments

We thank Michael Roberts and Sidney Kuo for preliminary observations that led us to search for electrical coupling in the DCN; Michael Bateschell and Ruby Larisch for help with mouse colony management and genotyping; Carolina Borges-Merjane for initially genotyping the *Thy1-ChR2* mice and providing cerebellum slices used in Supplemental Figure 2; Hsin-Wei Lu for writing the macros used to analyze the calcium imaging data; Sarah Foster for performing the ABR measurements. Kevin Bender, Will Giardino, and Nate Sawtell for critical comments on the manuscript. Funding was provided by NIH Grants R01DC004450 to L.O.T. and F31DC012222 to P.F.A. and P30 DC005983.

## References


1. Bell CC, Han V, Sawtell NB. Cerebellum-like structures and their implications for cerebellar function. Annu Rev Neurosci. 2008; 31:1–24. [PubMed: 18275284]
2. Dean P, Porrill J, Ekerot CF, Jörntell H. The cerebellar microcircuit as an adaptive filter: experimental and computational evidence. Nat Rev Neurosci. 2010; 11:30–43. [PubMed: 19997115]
3. Requarth T, Sawtell NB. Neural mechanisms for filtering self-generated sensory signals in cerebellum-like circuits. Curr Opin Neurobiol. 2011; 21:602–608. [PubMed: 21704507]
4. Oertel D, Young ED. What's a cerebellar circuit doing in the auditory system? Trends Neurosci. 2004; 27:104–110. [PubMed: 15102490]
5. Roberts MT, Trussell LO. Molecular layer inhibitory interneurons provide feedforward and lateral inhibition in the dorsal cochlear nucleus. J Neurophysiol. 2010; 104:2462–2473. [PubMed: 20719922]
6. Bennett MVL, Zukin RS. Electrical coupling and neuronal synchronization in the Mammalian brain. Neuron. 2004; 41:495–511. [PubMed: 14980200]
7. Hestrin S, Galarreta M. Electrical synapses define networks of neocortical GABAergic neurons. Trends Neurosci. 2005; 28:304–309. [PubMed: 15927686]
8. Christie MJ, Williams JT, North RA. Electrical coupling synchronizes subthreshold activity in locus coeruleus neurons in vitro from neonatal rats. J Neurosci. 1989; 9:3584–3589. [PubMed: 2795142]
9. Maher BJ, McGinley MJ, Westbrook GL. Experience-dependent maturation of the glomerular microcircuit. Proc Natl Acad Sci USA. 2009; 106:16865–16870. [PubMed: 19805387]
10. Bennett MV. Physiology of electrotonic junctions. Ann N Y Acad Sci. 1966; 137:509–539. [PubMed: 5229812]
11. Gibson JR, Beierlein M, Connors BW. Two networks of electrically coupled inhibitory neurons in neocortex. Nature. 1999; 402:75–79. [PubMed: 10573419]
12. Wouterlood FG, Mugnaini E, Osen KK, Dahl AL. Stellate neurons in rat dorsal cochlear nucleus studies with combined Golgi impregnation and electron microscopy: synaptic connections and mutual coupling by gap junctions. J Neurocytol. 1984; 13:639–664. [PubMed: 6481413]
13. Mann-Metzer P, Yarom Y. Electrotonic coupling interacts with intrinsic properties to generate synchronized activity in cerebellar networks of inhibitory interneurons. J Neurosci. 1999; 19:3298–3306. [PubMed: 10212289]
14. Leao RM, Li S, Doiron B, Tzounopoulos T. Diverse levels of an inwardly rectifying potassium conductance generate heterogeneous neuronal behavior in a population of dorsal cochlear nucleus pyramidal neurons. J Neurophysiol. 2012; 107:3008–3019. [PubMed: 22378165]
15. Davis KA, Young ED. Pharmacological evidence of inhibitory and disinhibitory neuronal circuits in dorsal cochlear nucleus. J Neurophysiol. 2000; 83:926–940. [PubMed: 10669505]
16. Molitor SC, Manis PB. Dendritic Ca2+ transients evoked by action potentials in rat dorsal cochlear nucleus pyramidal and cartwheel neurons. J Neurophysiol. 2003; 89:2225–2237. [PubMed: 12612001]
17. Tzounopoulos T, Kim Y, Oertel D, Trussell LO. Cell-specific, spike timing-dependent plasticities in the dorsal cochlear nucleus. Nat Neurosci. 2004; 7:719–725. [PubMed: 15208632]
18. Zhang S, Oertel D. Neuronal circuits associated with the output of the dorsal cochlear nucleus through fusiform cells. J Neurophysiol. 1994; 71:914–930. [PubMed: 8201432]
19. Dugué GP, et al. Electrical coupling mediates tunable low-frequency oscillations and resonance in the cerebellar Golgi cell network. Neuron. 2009; 61:126–139. [PubMed: 19146818]
20. Vervaeke K, et al. Rapid desynchronization of an electrically coupled interneuron network with sparse excitatory synaptic input. Neuron. 2010; 67:435–451. [PubMed: 20696381]
21. Gibson JR, Beierlein M, Connors BW. Functional properties of electrical synapses between inhibitory interneurons of neocortical layer 4. J Neurophysiol. 2005; 93:467–480. [PubMed: 15317837]
22. Ma WLD, Brenowitz SD. Single-neuron recordings from unanesthetized mouse dorsal cochlear nucleus. J Neurophysiol. 2012; 107:824–835. [PubMed: 22072506]

23. Rhode WS, Smith PH, Oertel D. Physiological response properties of cells labeled intracellularly with horseradish peroxidase in cat dorsal cochlear nucleus. J Comp Neurol. 1983; 213:426–447. [PubMed: 6300199]
24. Hancock KE, Voigt HF. Intracellularly labeled fusiform cells in dorsal cochlear nucleus of the gerbil. I. Physiological response properties. J Neurophysiol. 2002; 87:2505–2519. [PubMed: 11976387]
25. Merchan MA, Collia FP, Merchan JA, Saldana E. Distribution of primary afferent fibres in the cochlear nuclei. A silver and horseradish peroxidase (HRP) study. J Anat. 1985; 141:121–130. [PubMed: 4077711]
26. Arenkiel BR, et al. In vivo light-induced activation of neural circuitry in transgenic mice expressing channelrhodopsin-2. Neuron. 2007; 54:205–218. [PubMed: 17442243]
27. Hägglund M, Borgius L, Dougherty KJ, Kiehn O. Activation of groups of excitatory neurons in the mammalian spinal cord or hindbrain evokes locomotion. Nat Neurosci. 2010; 13:246–252. [PubMed: 20081850]
28. Ito T, Oliver DL. Origins of Glutamatergic Terminals in the Inferior Colliculus Identified by Retrograde Transport and Expression of VGLUT1 and VGLUT2 Genes. Front Neuroanat. 2010; 4:135. [PubMed: 21048892]
29. Mugnaini E. GABA neurons in the superficial layers of the rat dorsal cochlear nucleus: light and electron microscopic immunocytochemistry. J Comp Neurol. 1985; 235:61–81. [PubMed: 3886718]
30. Nagel G, et al. Channelrhodopsin-2, a directly light-gated cation-selective membrane channel. Proc Natl Acad Sci USA. 2003; 100:13940–13945. [PubMed: 14615590]
31. Mitchell SJ, Silver RA. Shunting inhibition modulates neuronal gain during synaptic excitation. Neuron. 2003; 38:433–445. [PubMed: 12741990]
32. Rubio ME, Juiz JM. Differential distribution of synaptic endings containing glutamate, glycine, and GABA in the rat dorsal cochlear nucleus. J Comp Neurol. 2004; 477:253–272. [PubMed: 15305363]
33. Isaacson JS, Scanziani M. How inhibition shapes cortical activity. Neuron. 2011; 72:231–243. [PubMed: 22017986]
34. Osen KK, Ottersen OP, Storm-Mathisen J. Osen: Colocalization of glycine-like and GABA-like… - Google Scholar. Glycine neurotransmission. 1990
35. Bell CC, Han VZ, Sugawara Y, Grant K. Synaptic plasticity in a cerebellum-like structure depends on temporal order. Nature. 1997; 387:278–281. [PubMed: 9153391]
36. Han VZ, Grant K, Bell CC. Reversible associative depression and nonassociative potentiation at a parallel fiber synapse. Neuron. 2000; 27:611–622. [PubMed: 11055442]
37. Bell CC, Caputi A, Grant K. Physiology and plasticity of morphologically identified cells in the mormyrid electrosensory lobe. J Neurosci. 1997; 17:6409–6423. [PubMed: 9236249]
38. Sawtell NB, Williams A. Transformations of electrosensory encoding associated with an adaptive filter. J Neurosci. 2008; 28:1598–1612. [PubMed: 18272681]
39. Hansel C, et al. alphaCaMKII Is essential for cerebellar LTD and motor learning. Neuron. 2006; 51:835–843. [PubMed: 16982427]
40. Szapiro G, Barbour B. Multiple climbing fibers signal to molecular layer interneurons exclusively via glutamate spillover. Nat Neurosci. 2007; 10:735–742. [PubMed: 17515900]
41. Mathews PJ, Lee KH, Peng Z, Houser CR, Otis TS. Effects of climbing fiber driven inhibition on Purkinje neuron spiking. J Neurosci. 2012; 32:17988–17997. [PubMed: 23238715]
42. Coddington LT, Rudolph S, Vande Lune P, Overstreet-Wadiche L, Wadiche JI. Spillover-mediated feedforward inhibition functionally segregates interneuron activity. Neuron. 2013; 78:1050–1062. [PubMed: 23707614]
43. Zhao S, et al. Cell type–specific channelrhodopsin-2 transgenic mice for optogenetic dissection of neural circuitry function. Nat Methods. 2011; 8:745–752. [PubMed: 21985008]
44. Kuo SP, Trussell LO. Spontaneous spiking and synaptic depression underlie noradrenergic control of feed-forward inhibition. Neuron. 2011; 71:306–318. [PubMed: 21791289]

45. Apostolides PF, Trussell LO. Rapid, Activity-Independent Turnover of Vesicular Transmitter Content at a Mixed Glycine/GABA Synapse. J Neurosci. 2013; 33:4768–4781. [PubMed: 23486948]

46. Bender KJ, Ford CP, Trussell LO. Dopaminergic modulation of axon initial segment calcium channels regulates action potential initiation. Neuron. 2010; 68:500–511. [PubMed: 21040850]

47. Devor A, Yarom Y. Electrotonic coupling in the inferior olivary nucleus revealed by simultaneous double patch recordings. J Neurophysiol. 2002; 87:3048–3058. [PubMed: 12037207]

48. Vervaeke K, Lorincz A, Nusser Z, Silver RA. Gap junctions compensate for sublinear dendritic integration in an inhibitory network. Science. 2012; 335:1624–1628. [PubMed: 22403180]

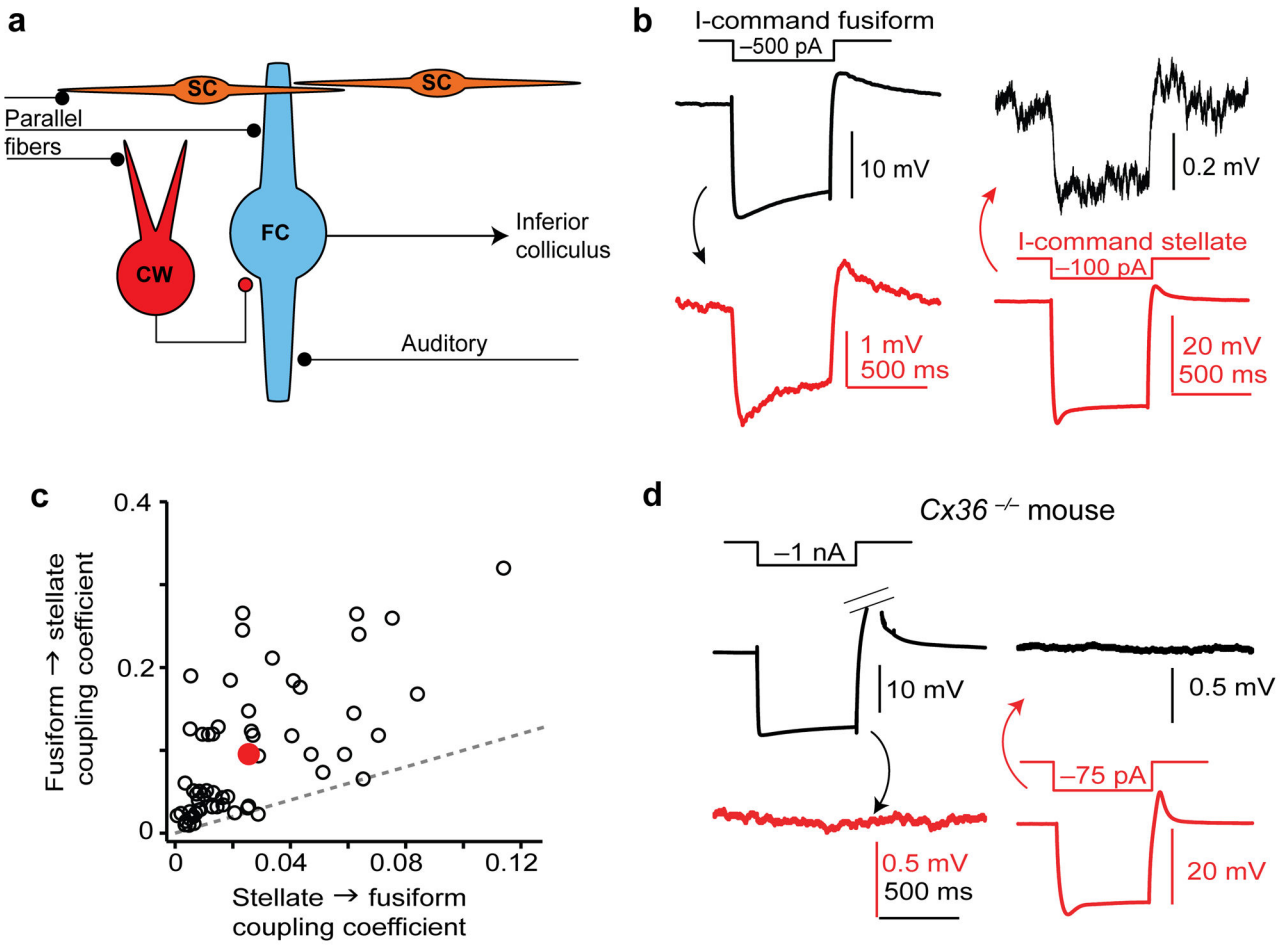


**Figure 1. Asymmetric electrical coupling between DCN fusiform and stellate cells**

a) Diagram of DCN circuitry. The excitatory projection neurons of the DCN (fusiform cells; FC), integrate excitatory auditory nerve and multisensory parallel fiber synapses[4]. Parallel fibers, but not auditory nerve fibers, impinge upon two distinct types of inhibitory interneurons: cartwheel cells (CW) and superficial stellate cells (SC).

b) Example average traces from an electrically-coupled fusiform/stellate pair. Negative current injection into the fusiform cell (black trace) causes the expected hyperpolarization. This causes a smaller voltage deflection with similar time course in the simultaneously recorded stellate cell (red trace, note the difference in scale). Similarly, hyperpolarizing the stellate cell causes a small voltage deflection in the fusiform cell.

c) Summary of coupling coefficients for 57 pairs similar to (b). Red point is average ± s.e.m of the data set, and dotted gray line represents the unity line. Almost all pairs fall above the unity line, showing that the coupling coefficient is stronger in the fusiform-to-stellate direction compared to vice versa.

d) Example average traces from a typical paired recording in a DCN slice from a Cx36−/− mouse. Color coding is similar to panel (b). Out of 60 attempts, only 3 pairs were connected.

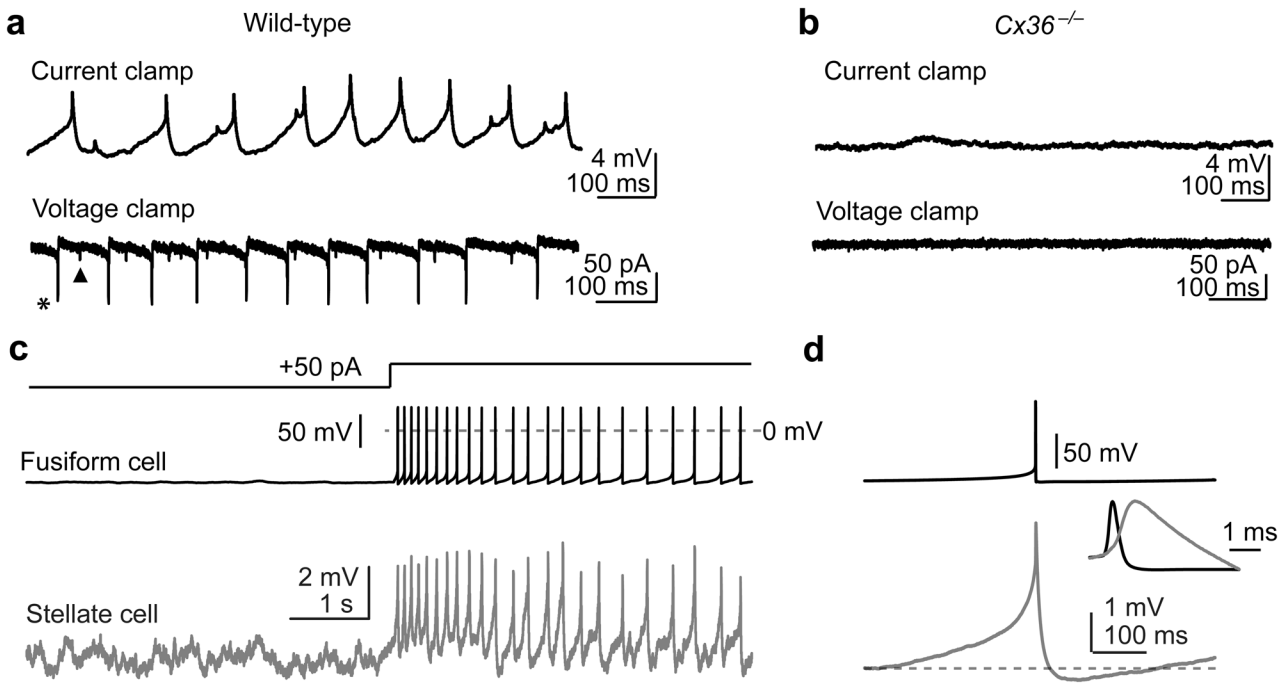


**Figure 2. Fusiform cells generate spikelets in electrically-coupled stellate cells**

a) Spontaneous spikelet activity in a single stellate cell recorded in current- and voltage-clamp (upper and lower traces, respectively). Recordings were performed in the presence glutamate, glycine and $GABA_A$ receptor blockers. Spikelet events with two distinct amplitudes are apparent (e.g., see asterisk and triangle), suggesting that at least two prejunctional fusiform cells with different coupling coefficients coupled to the same stellate cell.

b) Same experiment as (a), but in a *Cx36−/−* mouse. No spikelets were detected in knockout mice; (0/77 cells tested. $\chi^2(1)=72.4$, $p<0.0001$ compared to wild-type). Traces were recorded in the presence of synaptic blockers.

c) Paired recording from electrically-coupled fusiform and stellate cells (upper and lower traces, respectively). The fusiform cell was driven to spike by current injection. Notice the immediate onset, uniform amplitude, and lack of transmission failures of spikelets in the stellate cell.

d) Averages (acquisition triggered by detection of the prejunctional spike) from the same pair as in (c). Only spikes that occurred more than 300 ms apart were included in the average, to highlight the time course of the depolarizing and hyperpolarizing phases of the spikelet waveform. Inset shows the spikelet rising phase on a fast time base and normalized to the peak of the prejunctional spike, highlighting that spikelets rise before the downswing of the fusiform cell action potential.

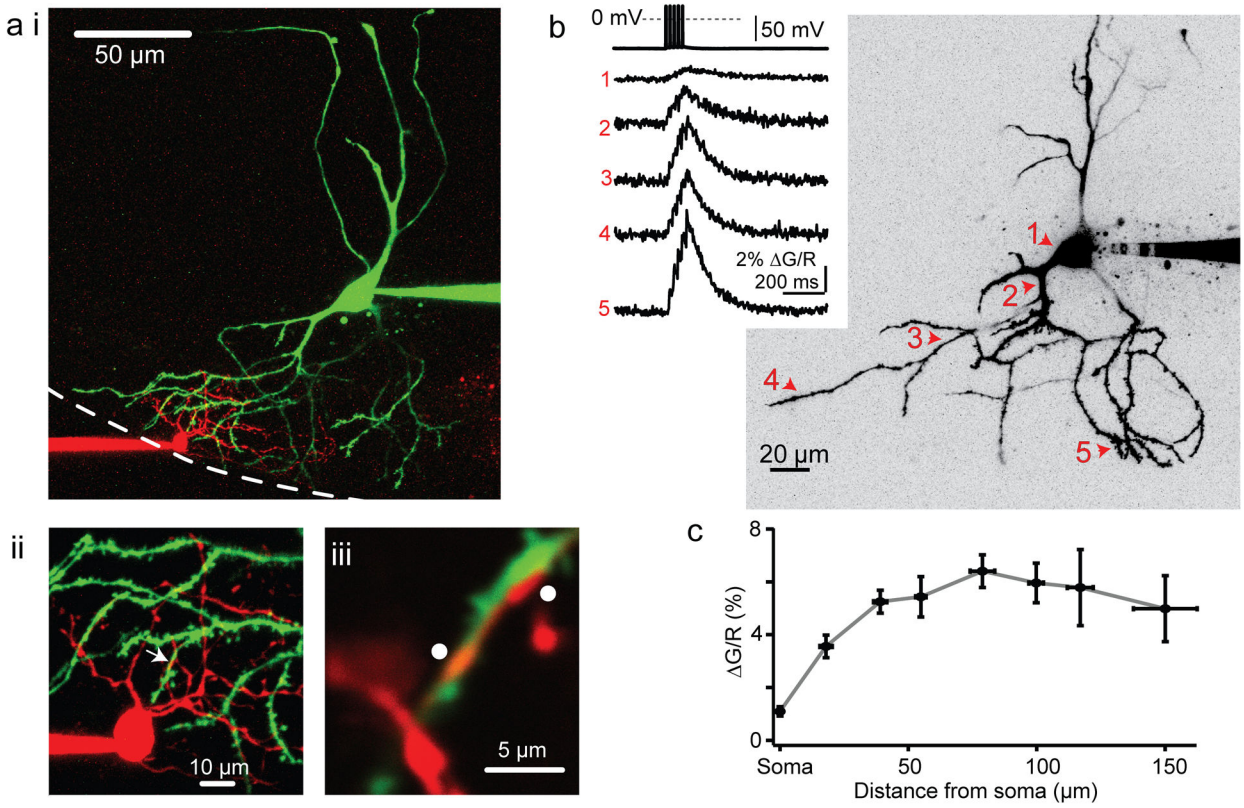


**Figure 3. Fusiform cell action potentials propagate into the distal apical dendrites**

a-i) 2-photon maximum-intensity z-stack from the example in Figure 1b. The stellate and fusiform cells are filled with Alexa594 (red) and Alexa488 (green) dyes, respectively. Dotted white line represents the approximate ependymal border of the DCN. Stellate cell processes do not extend into the cell body layer, whereas fusiform cell processes span the entire length of the DCN.

a-i) A maximal intensity z-stack at higher magnification from the same pair.

a-iii) High magnification, single optical section of the area denoted by the white arrow in panel (b), showing a high degree of overlap between the stellate and fusiform cell processes (white dots).

b) Right: Maximum intensity 2-photon z-stack from a representative fusiform cell showing line scan locations during the $Ca^{2+}$ imaging experiment. Left: Example sweeps of action potential-evoked Fluo-5f $Ca^{2+}$ transients (5 spikes, 50 Hz) recorded at the corresponding dendritic locations marked in the z-stack on the left. Each trace is an average of 20–25 trials.

c) Absolute ΔG/R plotted as a function of approximate distance from the soma. Response amplitudes remain relatively constant along the dendrite. Each data point represents mean values ± s.e.m. from 3 to 6 individual cells.

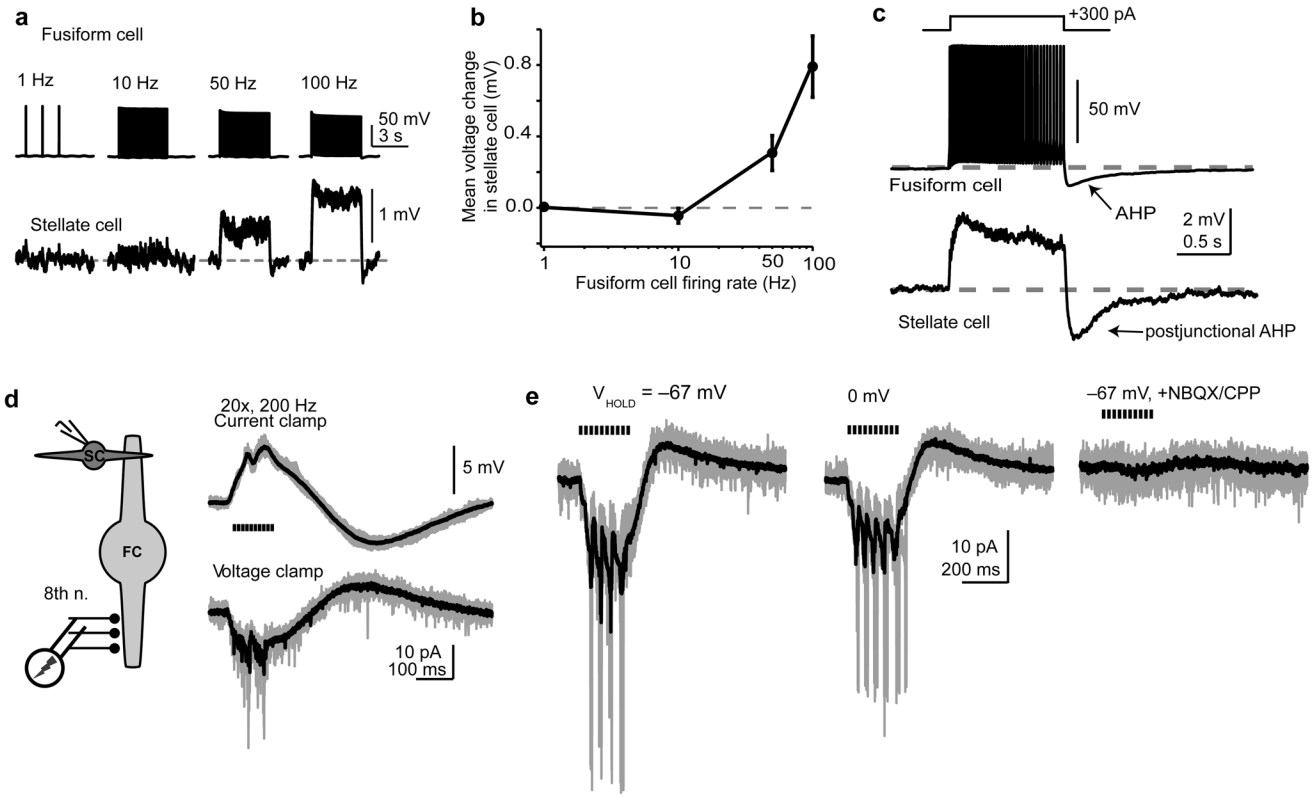


**Figure 4. Control the stellate cell membrane potential by fusiform cells and auditory nerve activity**

a) Upper traces: fusiform cell spikes evoked at different frequencies (single trials). Lower traces: averages of multiple trials in an electrically-coupled stellate cell.

b) Summary data (n=9) showing stellate cell mean voltage change ±s.e.m. from baseline vs. fusiform cell spike frequency.

c) Current injection in a fusiform cell triggered high-frequency firing followed by post-train AHP upon stimulus offset (upper trace). Simultaneously recorded, postjunctional stellate cell (lower trace) was transiently depolarized above baseline) during fusiform cell spiking and hyperpolarized by the AHP upon stimulus termination. Top trace: single trial, bottom trace: average of eight sweeps.

d) Activation of auditory nerve elicits biphasic signals in stellate cells. Left panel: A stimulating electrode was placed in the ventral cochlear nucleus (VCN) >600 μm from the recorded cell in DCN. Recording made in the presence of 1 μM strychnine/10 μM SR95531. Right panel: Stellate cell recorded in current or voltage clamp (upper and lower traces, respectively) during stimulation of the VCN (20 shocks at 5-ms intervals). In current clamp, negative bias current (−30 pA) was injected to prevent spike generation.

e) VCN stimuli (10 shocks at 50 Hz) were delivered while the cell was clamped at −67 mV or 0 mV. Little difference was seen in response amplitude at the two potentials. Lower trace: 10 μM NBQX, 5 μM CPP eliminated the response, as expected for glutamatergic transmission from auditory nerve. For panels d+e, gray traces are 5 consecutive trials, and black traces are averages of 12–31 trials. Stimulus artifacts were blanked.

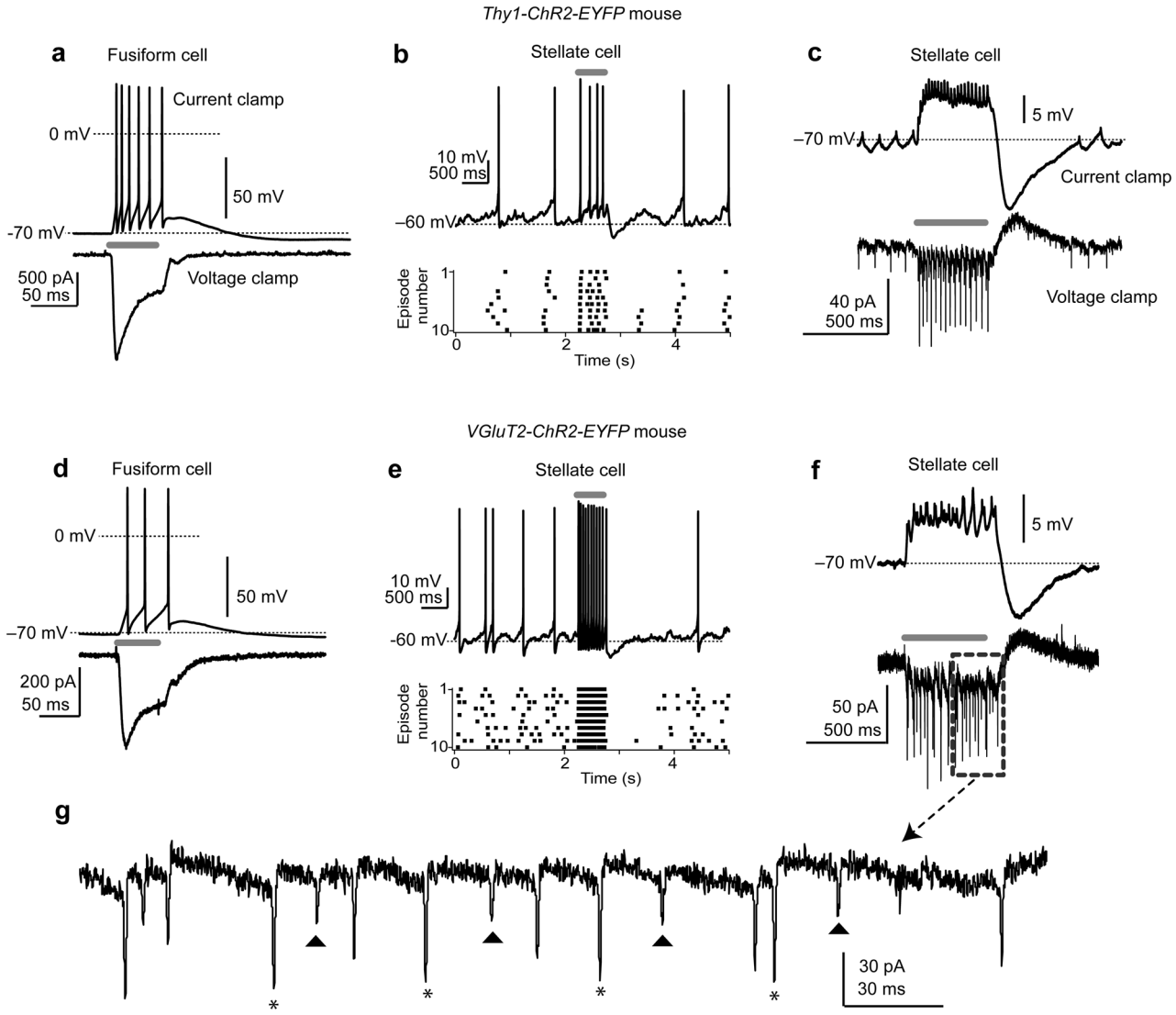


**Figure 5. Optogenetic activation of fusiform cells depolarizes stellate cells**

a) In a *Thy1-ChR2-EYFP* fusiform cell, light stimuli (50 ms; blue bar) generate spikes in current-clamp (upper traces) and photocurrents in voltage clamp (lower traces). Top trace: single trial, lower trace: average of multiple trials.

b) Top: Current-clamp recording from a stellate cell in a *Thy1-ChR2-EYFP* mouse (zero bias current). A 500-ms light stimulus (gray bar) causes an immediate increase in spike frequency. Lower panel: Raster plot of ten trials, highlighting the increase in spike rate upon optogenetic stimulation of fusiform cells. Similar results obtained in 18/19 stellate cells.

c) Stellate cell in a *Thy1-ChR2-EYFP* mouse (different cell from b). Top trace: Current clamp, −25 pA bias current injected to hyperpolarize the cell and prevent spike generation. Light flash (400 ms) causes spikelets riding atop a steady-state depolarization, followed by an AHP at light offset. Note similarity to the traces in Figure 4c. Lower trace: Same stimulus delivered when the cell is voltage-clamped at −70 mV causes a barrage of fast inward spikelets, followed by a slow outward current upon stimulus offset. Traces are single trials.

d) A fusiform cell in a *VGluT2-ChR2-EYFP* mouse. Similar to Thy1-ChR2 mouse in panel (a), light (50 ms) drives spikes and induces photocurrents.
e) Current-clamp recording from a stellate cell in the *VGluT2-ChR2-EYFP* mouse. The experiment and panel layout as in (b).
f) A stellate cell in a *VGluT2-ChR2* mouse showing that light stimuli cause depolarizations and inward currents as in the *Thy1-ChR2* mouse.
g) Enlargement of the area denoted by the gray dashed rectangle in (f). Note presence of spikelets with distinct amplitudes (denoted by triangles and asterisks), suggesting coupling to at least two fusiform cells with different coupling coefficients.

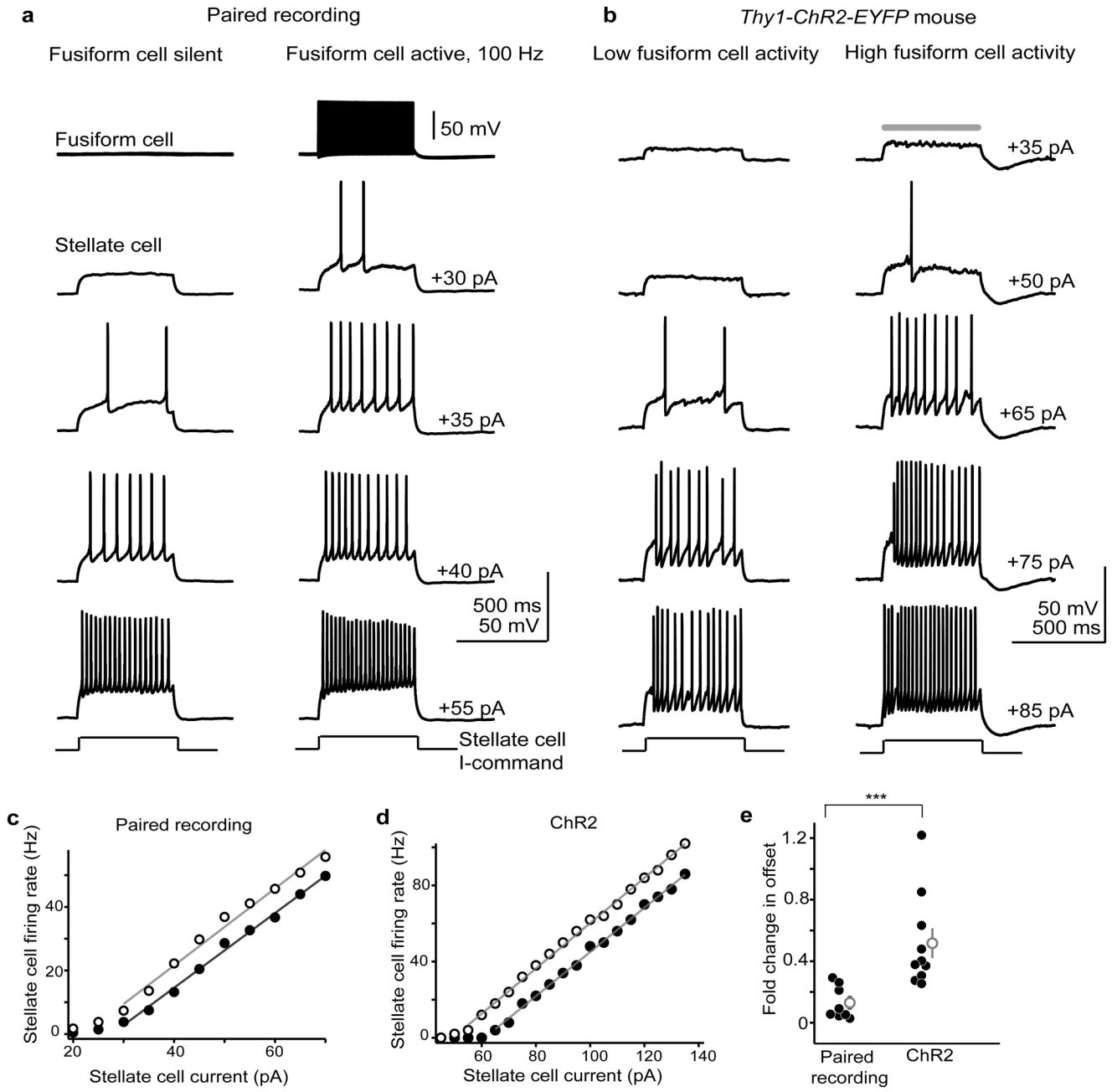


**Figure 6. Fusiform cells control the spike rate of stellate cells**

a) Single trials from an electrically-coupled fusiform-stellate cell pair. The stellate cell was depolarized with step pulses of increasing positive current (2.5–5 pA intervals; 500 ms duration) in absence or with simultaneous 100 Hz activity in the fusiform cell (left and right columns, respectively). Activity in the prejunctional fusiform cell increases the total number of spikes generated in the stellate cell with intermediate current steps.

b) Example single trials from a stellate cell in a *Thy1-ChR2* mouse. Traces show stellate cell spikes evoked by positive current injection (500 ms) with (right) and without (left) concurrent blue light flashes (gray bar, 500 ms) to activate prejunctional fusiform cells.

c) Input/output curve for the pair in (a). Spike frequency (y-axis) is plotted as a function of current injection. Solid points represent values while the prejunctional cell was silent; open points are with concurrent prejunctional fusiform cell activity. The gray lines are linear fits to the non-zero portions of the data.

d) Same as panel c, but for the ChR2 experiment. The open and filled circles represent the input-output curves of the example cell in (b) with and without simultaneous blue light flashes, respectively.

e) Summary graph plotting the normalized change in offset (x-intercept) due to fusiform cell activity in paired recordings and ChR2 experiments. Gray points are mean ± s.e.m.. Asterisks denote statistical significance. Optogenetic stimulation caused a 3.7-fold greater shift in offset compared to paired recordings ($t(16)=3.4$, $p=0.004$, unpaired t-test).

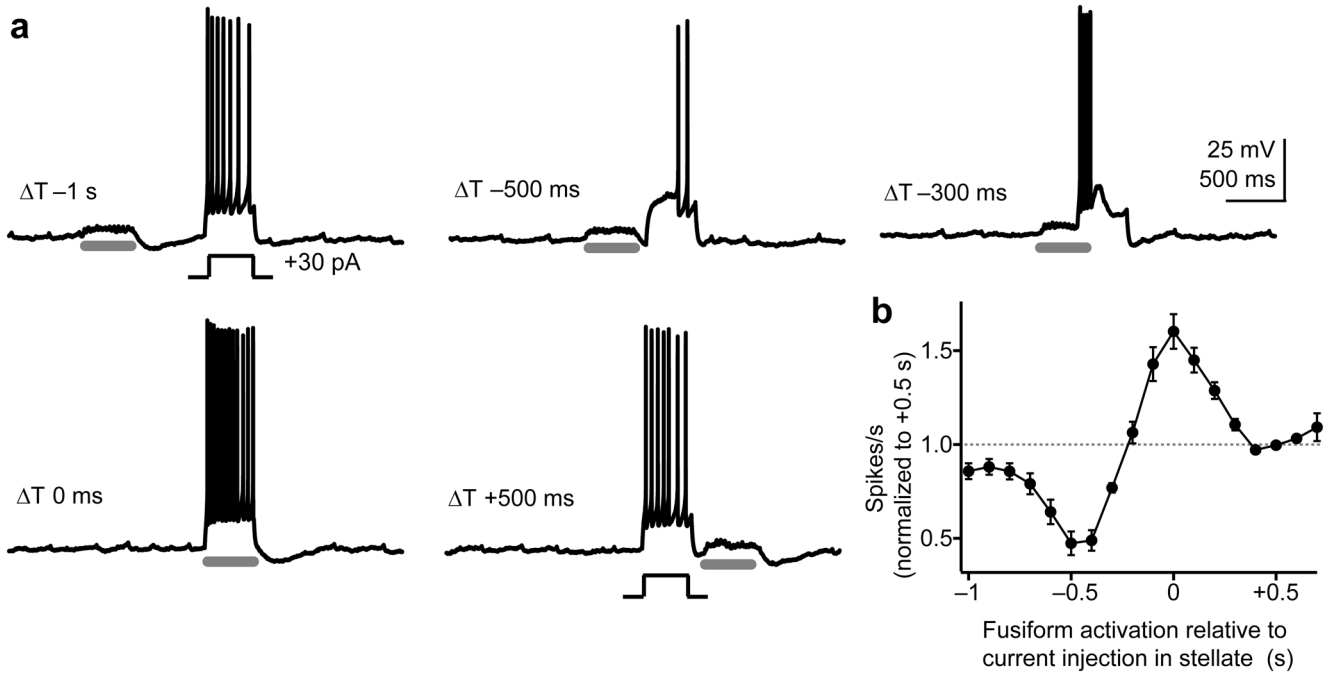


**Figure 7. The timing of fusiform cell activity bi-directionally controls stellate cell spike output**

a) Single trials from a stellate cell in a *VgluT2-ChR2* mouse where the cell was transiently driven to spike via positive current injection (400 ms). Prejunctional fusiform cells were activated by blue light (gray bars, 400 ms) at various times relative to the current step in the stellate cell. Negative bias current was used to prevent spontaneous firing.

b) Summary graph from 13 stellate cells in ChR2 mice plotting normalized spikes/s as a function of flash timing relative to stellate cell current injection. The data (means ± s.e.m.) are normalized to the +500 ms data point, where the light flash (and thus, fusiform cell activation) occurred *after* the current step in the stellate cell.

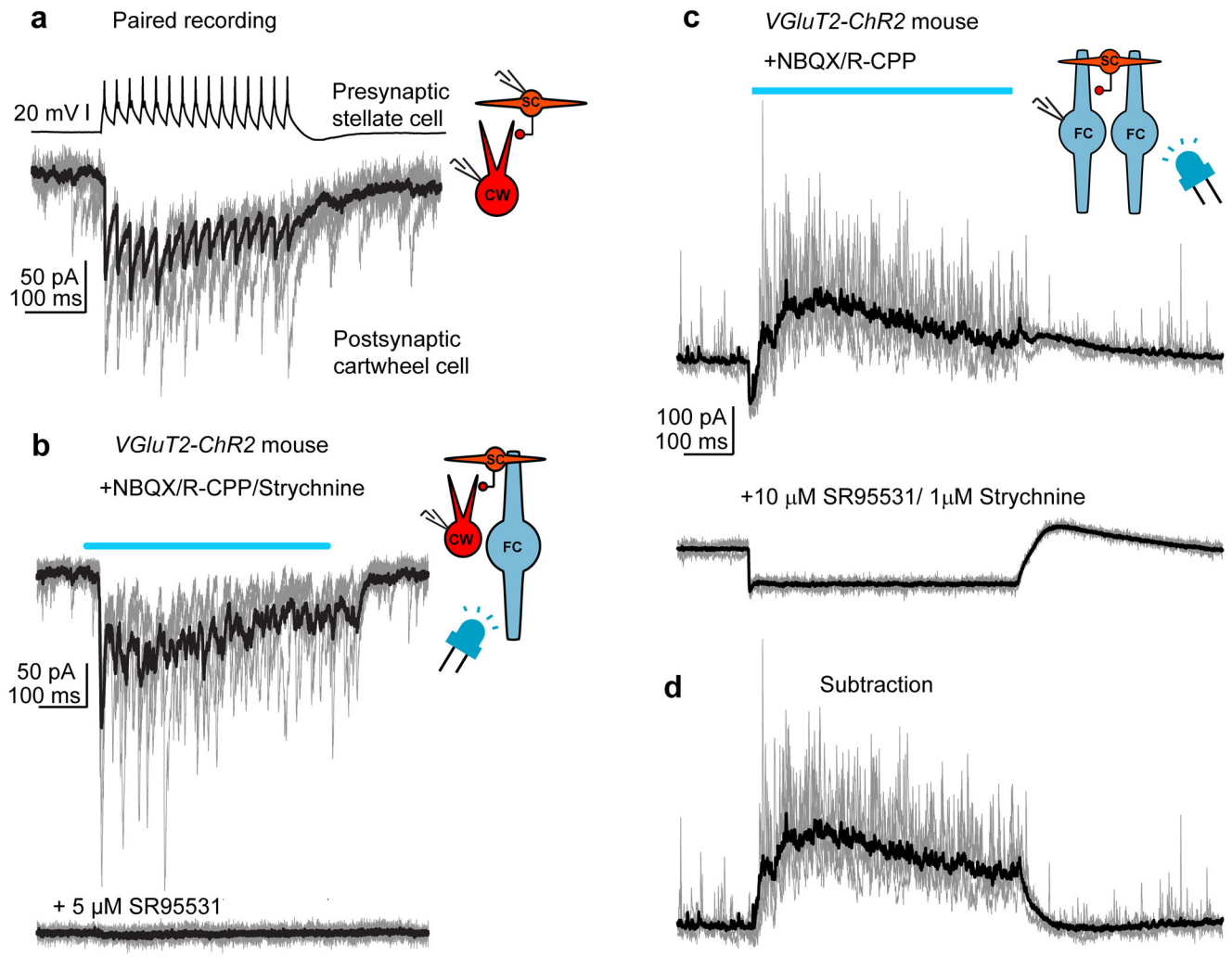


**Figure 8. Fusiform cells generate inhibition in the DCN**

a) Paired recording between a presynaptic stellate and postsynaptic cartwheel cell. GABAergic transmission isolated with glutamate and glycine receptor blockers. 15 action potentials were elicited at 50 Hz in the stellate cell, resulting in a time-locked series of IPSCs in the postsynaptic cartwheel cell. IPSCs are inward as the cartwheel cell is recorded with a $Cl^-$ rich internal solution. Gray traces are 4 single sweeps, black is an average of 20 trials.

b) A cartwheel cell in a *VGluT2-ChR2* mouse. Top trace: Optogenetic stimulation of fusiform cells, denoted by the blue line, results in a barrage of IPSCs in the cartwheel cell. Lower trace: The $GABA_A$ receptor antagonist SR95531 blocks the optogenetically-evoked IPSCs. Gray traces are 4 single sweeps, black is an average of 10 trials in each condition.

c) Example recording from a fusiform cell in a *VGluT2-ChR2* mouse. The cell is voltage-clamped at 0 mV, generating a net outward driving for $Cl^-$ currents. Upper panel: Activating neighboring fusiform cells via blue light stimuli (500 ms) causes a powerful increase in IPSC frequency. Lower panel: IPSCs are blocked by the addition of $GABA_A$/glycine receptor blockers SR95531 and strychnine, revealing an inward photocurrent during the

light stimulus. Gray traces are 5 consecutive trials. Black traces are an average of 20 to 23 trials.

d) Same example traces as those in the upper panel of (c), but with the average photocurrent digitally subtracted. Thus, activation of neighboring fusiform cells causes an inhibitory outward current for the duration of the light stimulus.